Mar Biotechnol (2015) 17:130–143
DOI 10.1007/s10126-014-9601-0

ORIGINAL ARTICLE

Recombinant Production and Characterization of a Highly Active Alkaline Phosphatase from Marine Bacterium *Cobetia marina*

Vasily Golotin · Larissa Balabanova · Galina Likhatskaya · Valery Rasskazov

Received: 17 August 2013 / Accepted: 7 August 2014 / Published online: 27 September 2014

Abstract The psychrophilic marine bacterium, *Cobetia marina*, recovered from the mantle tissue of the marine mussel, *Crenomytilus grayanus*, which contained a gene encoding alkaline phosphatase (AP) with apparent biotechnology advantages. The enzyme was found to be more efficient than its counterparts and showed k_{cat} value 10- to 100-fold higher than those of all known commercial APs. The enzyme did not require the presence of exogenous divalent cations and dimeric state of its molecule for activity. The recombinant enzyme (*Cm*AP) production and purification were optimized with a final recovery of 2 mg of the homogenous protein from 1 L of the transgenic *Escherichia coli* Rosetta(DE3)/Pho40 cells culture. *Cm*AP displayed a half-life of 16 min at 45 °C and 27 min at 40 °C in the presence of 2 mM EDTA, thus suggesting its relative thermostability in comparison with the known cold-adapted analogues. A high concentration of EDTA in the incubation mixture did not appreciably inhibit *Cm*AP. The enzyme was stable in a wide range of pH (6.0–11.0). *Cm*AP exhibited its highest activity at the reaction temperature of 40–50 °C and pH 9.5–10.3. The structural features of *Cm*AP could be the reason for the increase in its stability and catalytic turnover. We have modeled the *Cm*AP 3D structure on the base of the high-quality experimental structure of the close homologue *Vibrio* sp. AP (VAP) and mutated essential residues predicted to break Mg^{2+} bonds in *Cm*AP. It seems probable that the intrinsically tight binding of catalytic and structural metal ions together with the flexibility of intermolecular and intramolecular links in *Cm*AP could be attributed to the adapted mutualistic lifestyle in oceanic waters.

V. Golotin · L. Balabanova (✉) · G. Likhatskaya · V. Rasskazov
G.B. Elyakova Pacific Institute of Bioorganic Chemistry, Far-Eastern Branch of Russian Academy of Sciences, Prospect 100-letya Vladivostoka, 159, Vladivostok, Russian Federation
e-mail: balaban@piboc.dvo.ru

Keywords Biochemical properties · Expression · Catalytic efficiency · Homology modeling · Purification · Site-directed mutagenesis

Introduction

Phosphatase is an important enzyme in recycling phosphate in marine environments as well as within living cells. Its distribution is dependent on environmental factors such as phosphate availability, dominant habitants, water depth, salinity, temperature, and the internal ratio of nitrogen to phosphorus in higher organisms and microbial communities (Hoppe 2003). Interestingly, high alkaline phosphatase (AP) activity occurs in eutrophic or deep water in the presence of relatively high phosphate concentrations (Dell'Anno and Danavaro 2005). Analysis of a marine community revealed that bacteria attached to particulates or associated with another marine habitat were frequently stronger producers of APs than free-living bacteria (Ivanova et al. 2005). In fact, the bacterial APs can account for a relatively higher uptake of P_i from degradable organic matters (Paerl and Merkel 1982). The activity of constitutive APs that is often irrespective of the environmental phosphate concentration is the result of AP expression under symbiotic conditions, and the AP may have a role in nutrient exchange with host organisms rather than in nutrient uptake from the host tissues (Aono et al. 2004; Plisova et al. 2005). Thus, the marine bacterium *Cobetia marina* strain KMM 296 (Collection of Marine Microorganisms PIBOC FEB RAS), which was recovered from mussels, appeared to have metabolic specialization by producing a highly active extracellular AP (specific activity of 15,000 U/mg protein). This enzyme may play an active role in the invertebrate's shell mineralization during seasonal phosphate diminution, when the bone-like exoskeleton is broken down and continuously renewed (Leveque et al. 2004; Plisova et al. 2005; Dorozhkin 2009).

The strain *C. marina* KMM 296 did not require Na^+ for growth and could grow at the wide range of temperatures from 4 to 42 °C, which is in contrast to other seawater isolates of *Halomonas*-like strains (Ivanova et al. 2005). The AP from *C. marina* KMM 296 (*Cm*AP) was found to be relatively heat-stable for a psychrophile and functioned independent of extraneous bivalent metal ions and high inorganic phosphorus (P_i) or EDTA concentrations in the incubation medium (Plisova et al. 2005). Only a limited number of marine bacterial APs have been reported to be similar to *Cm*AP in that they have unusual structures and cold-adapted properties such as a low thermostability and high catalytic efficiency (Plisova et al. 2005; Nasu et al. 2012). There are a few experimentally studied marine bacterial cold-active APs from Antarctic strains (Kobori et al. 1984; Rina et al. 2000), *Vibrio* sp. G15-21 (Hauksson et al. 2000), *Shewanella* sp. (Murakawa et al. 2002), *Shewanella* sp. SIB1 (Suzuki et al. 2005), *Holomonas* sp. 593 (Ishibashi et al. 2005) and *C. marina* KMM 296 (Plisova et al. 2005). All of these enzymes belong to γ-Proteobacteria, with the exception of an unidentified Antarctic bacterium species TAB5 (Rina et al. 2000).

We have developed a method for the production of a highly active recombinant AP of *C. marina* (*Cm*AP) in *Escherichia coli*. To gain insight into the function of this unique enzyme, we report the results of its biochemical and catalytic characterization, site-specific mutagenesis experiments and molecular homology modeling data. In addition, we show the distinctive features of *Cm*AP that make it important to the commercial application.

Materials and Methods

Bacterial Strains and Plasmids

C. marina KMM 296 (Collection of Marine Microorganisms PIBOC FEB RAS) cells were the source of chromosomal DNA for the *Cm*AP gene isolation. The strain was cultivated by the shake-flask method in a 1,000-mL Erlenmeyer flask on a rotary shaker (160 rpm) at 25 °C for 36 h. The bacterial cells were grown in a culture medium containing 5 g peptone, 2.5 g yeast extract, 1 g glucose, 0.05 g Mg_2SO_4, and 0.2 g K_2HPO_4 in 750 mL seawater and 250 mL distilled water. *E. coli* DH5α and Rosetta(DE3) (Novagen) cells were used as hosts for propagation and expression of the recombinant plasmid Pho40, respectively. The recombinant plasmid 40Ph of 7,699 bp for the synthesis of the recombinant protein *Cm*AP consists of the NcoI/EcoRI-fragment of plasmid pET-40b (+) (Novagen) and the gene corresponding to the mature *Cm*AP open reading frame.

Recombinant DNA Technique

For the *Cm*AP gene amplification, Encyclo Taq Polymerase (Eurogen) and the gene-specific upstream primer, 5′-TTAA CCATGGCAGAGATCAAGAATGTCATTCTGAT-3′, and the downstream primer, 5′-TTAAGAATTCCTTCGCTACC ACTGTCTTCAGATACTGTCC-3′, were used. For preparing the *Cm*AP mutants, the single amino acid substitutions Asp12Gly, Asp64Gly, Asp443Gly, Thr118Gly, Glu268Gly, Asp315Gly, Trp274Gly, His316Gly, and Asp273Gly were introduced into the 35-mer amino-modified oligonucleotides complemented to both DNA chains used in polymerase chain reaction (PCR). Then, the resultant PCR products appeared for both as DNA matrix and primers in equivalent ratio for the next PCR. The resultant mutant gene was amplified with the gene-specific primers as described above. PCR was carried out in automatic amplifier Eppendorf. Restriction endonucleases and T4 DNA ligase were purchased from Fermentas. The PCR product and plasmid pET-40b (+) restricted were purified on agarose gel using a Qiagen column. The recombinant insert of the resultant plasmid Pho40 was sequenced using the automated PE/ABI 310 DNA sequencer and the PE/ABI-ABI PRISM BigDye Terminator cycle sequencing Ready Reaction Kit (PE Applied Biosystems). Preparation of *E. coli* competent cells and heat shock transformation were carried out according to the standard method (Sambrook et al. 1989). All biochemicals and reagents were purchased from Fermentas and Sigma-Aldrich.

Recombinant AP Expression

For the expression of *Cm*AP and its mutants Asp12Gly, Asp64Gly, Asp443Gly, Thr118Gly, Glu268Gly, Asp315Gly, Trp274Gly, His316Gly, and Asp273Gly, the *E. coli* Rosetta(DE3) cells that transformed with the recombinant plasmid Pho40 (*E. coli* Rosetta(DE3)/Pho40) were grown on lysogeny broth (LB) plates containing 25 mg/mL kanamycin overnight at 37 °C. A single colony was selected and grown at 200 rpt in 20 mL of LB with 25 mg/mL kanamycin 37 °C for 12 h and then transferred to 1 L of fresh LB with 25 mg/mL kanamycin. When the cell density reached an A600 of 0.6–0.8, 0.2 mM IPTG was added to induce the expression of the protein, and the incubation continued at 16 °C up to 12 h at 200 rpt. The *E. coli* Rosetta(DE3) cells were transformed with the pET-40b (+) plasmid as a control.

Recombinant AP Purification

All purification steps were carried out at 6 °C. After harvesting, the *E. coli* Rosetta(DE3)/Pho40 cells were resuspended in 150 mL of a buffer containing 0.05 M Tris–HCl, pH 8.6, and 0.01 % NaN_3 (buffer A) and disintegrated by ultrasonic treatment, then centrifuged at 10,000*g* for 30 min. The supernatant

was applied to a column (4×25 cm) of DEAE-52 cellulose (Whatman). Elution of the protein was performed by a gradient of NaCl concentration (0.05–0.38 M) in 18 column volumes (CV) of the buffer A. The enzymatically active fractions were collected and applied onto a column (1×2.5 cm) of Ni-agarose (Qiagen). Elution of the protein was carried out by buffer B (50 mM Tris–HCl, pH 8.6, 50 mM EDTA, 0.01 % NaN_3). The active fractions were collected and desalted by using a DEAE-Toyopearl 650 M (Toyo Soda) column (0.7×2.5 cm) and then incubated with enterokinase (Invitrogen) at 21 °C for 15 h. Then, the protein solution was applied onto a gel filtration column (1.5×170 cm) of Sephacryl S-100HR (Sigma) with the buffer C (50 mM Tris–HCl, pH 8.6, 100 mM NaCl, 0.01 % NaN_3) at a flow of 0.13 mL/min, +6 °C. All purification steps were evaluated by sodium dodecyl sulfate polyacrylamide gel electrophoresis (SDS-PAGE). The concentration of protein was determined according to Bradford (1976).

Enzyme Activity Assay

The standard assay for AP activity was carried out at 37 °C using 2 mM *p*-nitrophenylphosphate (pNPP) (Sigma Chemical Co.) in 0.1 M Tris–HCl buffer, pH 9.0, containing 0.2 M KCl. The release of *p*-nitrophenol (ε=18.5 mM/cm) was monitored at 405 nm. One unit of AP activity was defined as the quantity of the enzyme required to release 1.0 μmol of *p*-nitrophenyl from pNPP in 1 min. The specific activity was calculated as units per 1 mg of protein.

Kinetic Parameters

Kinetic parameters of hydrolyzing reaction were verified by plotting reaction rates against concentrations of pNPP 0.1–0.6 and 0.2–3.0 mM for the enzyme assay in 0.1 M Tris–HCl buffer, 0.2 M KCl, at pH 8.0 and 10.3, respectively. For the enzyme activity assay carried out in 1 M diethanolamine (DEA) buffer at pH 8.0 and 10.3, the concentrations of pNPP were in the range of 0.1–1.0 and 0.5–15 mM, respectively. The K_m, V_{max}, and k_{cat} values were determined by nonlinear regression analysis of the plots by using Origin 8.1. The extinction coefficients for *p*-nitrophenol were measured to be 18.5 (0.1 M Tris–HCl) and 18.7 mM/cm (1 M DEA) at pH 10.3 and 17.7 mM/cm at pH 8.0 in both buffers. All enzyme activity assays were carried out at 25 °C.

Molecular Mass Determination

The molecular size of the active enzyme was determined by gel filtration on a column of Sephacryl S-100HR (Sigma) (1.5×170 cm) in 50 mM Tris–HCl, pH 8.6, and 100 mM NaCl at a flow of 0.13 mL/min at 6 °C and calibrated using Bio-Rad standard molecular weight markers: thyroglobulin bovine (670 kDa), γ-globulin bovine (158 kDa), ovalbumin chicken (44 kDa), myoglobin horse (17 kDa), and vitamin B12 (1.35 kDa). The molecular mass of the enzyme was determined by 12.5 % PAGE. The protein preparation was mixed with Laemmli sample buffer in the absence of β-mercaptoethanol and with or without heat treatment at 95 °C and then applied to PAGE. The gels were stained according to Laemmli (1970). PAGE for the native *Cm*AP was carried out in the absence or presence SDS in concentration from 0.1 to 1 % without heat treatment. The "native" gels were cased over with the standard enzyme assay buffer containing 2 mM pNPP and stained for AP. Both PAGEs were performed at 25 °C.

Temperature and pH Stability Assay

The apparent temperature optimum for the enzyme-specific activity was determined by measuring the activity at different temperatures in standard enzymatic assay buffer for 30 min. The reaction temperatures ranged from 20 to 65 °C. The half-life of the enzyme was determined as the temperature and the time required to half the initial activity. The enzyme was incubated at the appropriate temperatures for 10-min intervals, cooled in the ice bath, and the residual activity was measured using the standard enzyme assay at 25 °C for 30 min.

The effects of pH values on activity and stability of the enzyme were determined by measuring the activities at the different pH values by the standard method of the enzyme activity assay. The pH ranges varied from 4.0 to 11.0. The buffers used were 0.03 M $NaCOOH_3$ (4.0–6.0), 0.05 M Tris–HCl (7.0–9.0), 0.1 M $NaHCO_3$ (9.0–11.0), and 0.1 M glycine (9.0–11.0). The pH stability was evaluated by pre-incubation of the enzyme in each buffer for 1/2, 2, and 5 h and the residual activity measured using the standard enzyme assay.

Effects of Chemicals

The effects of Mg^{2+} on the temperature stability were evaluated by adding 2–10 mM $MgCl_2$ to the enzyme pre-incubation mixture containing 50 mM Tris–HCl, pH 8.6, at each temperature for up to 5 h, then the remaining activity assayed by the standard method. The effect of EDTA on the activity and stability of the enzyme was evaluated by adding it to the standard reaction mixture for the enzyme activity assay at 37 °C for 30 min or pre-incubating the enzyme mixture containing 50 mM Tris–HCl, pH 8.6, with EDTA in different concentrations (0–100 mM), and then the remaining activity was assayed by the standard method. The effects of KCl, NaCl, and SDS on the activity of the enzyme were evaluated by adding the chemicals in the standard incubation mixture at different concentrations.

Metal Ion Analysis

For atomic absorption analysis, samples were desalted by gel filtration on a Sephadex G-25 column in Tris–HCl (pH 8.6)

buffer. The concentration of protein for analysis was 0.22 mg/mL, and samples were acidified with 1 M HCl prior to injection. Shimadzu 6800 (Japan) atomic absorption spectrometer was employed to measure bivalent metal ions in flame atomization mode.

Statistics

All values presented in this article are representative of at least three independent experiments. Data were analyzed using the Student's *t* test of the SigmaPlot 2000 version 6.0 program (SPSS Inc.). Differences from controls were considered significant at $p \leq 0.05$.

Molecular Modeling

The target-template alignment customization of the modeling process and 3D model building of *Cm*AP were carried out by the molecular graphics package Molecular Operating Environment version 2012.10 (Chemical Computing Group Inc., 1010 Sherbooke St. West, Suite #910, Montreal, QC, Canada, H3A 2R7, 2012). The evaluation of structural parameters, contact structure analysis, physicochemical properties, and molecular docking and visualization of the results were carried out by the use of the modules of MOE v.2012. The molecular dynamics simulations were performed by using GROMACS v. 4.6.3 (Van der Spoel et al. 2005, 2013; Hess et al. 2008). The calculations of the pKa values were performed by PROPKA server (http://propka.ki.ku.dk/) (Li et al. 2005; Olsson et al. 2011).

Estimates of binding strengths and specificities were carried out for different ion types. Knowledge-based potentials for interactions of all nonhydrogen protein atoms with inorganic ions were obtained from a training set of Protein Data Bank (PDB) structures using Monte Carlo reference state (MCRS) as described previously (Rahmanov et al. 2010). The structure was covered by a cubic grid with a step of 0.2 Å and at grid nodes not sterically clashing with protein atoms. Probabilities of occupancy were calculated for different ions as a sum of inputs from all neighboring protein atoms. Conjugate gradient descent procedure was followed by random walk of decreasing steps to obtain the final maxima of ion probabilities of occurrence.

Results

Expression and Purification of *Cm*AP

The *Cm*AP production reached 2 mg of the final yield of the functionally active protein from 1 L of the *E. coli* Rosetta(DE3)/Pho40 cells culture carrying the expression recombinant vector 40Ph (Table 1). The optimal concentration of IPTG and temperature of the strain cultivation for the *Cm*AP expression were 0.2 mM and 16 °C, respectively, for 12 h (data not shown). At the final step of purification, SDS-PAGE showed a single band of the protein with a molecular mass of approximately 55,000 Da corresponding to the mature *Cm*AP (Fig. 1). The presence of 5 % mercaptoethanol, 10 % SDS, and 10 mM dithiothreitol or 6 M urea in the sample buffer did not have any effect on electrophoretic mobility of the *Cm*AP band (data not shown).

Effect of pH and Temperature on *Cm*AP Activity and Stability

The recombinant *Cm*AP had optimal activity at pH 9.5–10.3 in 1 M DEA buffer with 15–20 mM of *p*NPP. *Cm*AP was stable at pHs between 6.0 and 11.0 but was gradually inactivated at pHs below 6.0 (Fig. 2). *Cm*AP was also gradually inhibited when the enzyme was exposed at above pH 8.5 maintained by 0.1 M glycine (Fig. 2).

*Cm*AP had temperature optimums at 40 °C and 50 °C for the manifestation of its higher specific activity (Fig. 3). *Cm*AP was a relatively heat-stable enzyme with a half-life of 27 min at 40 °C and 16 min at 45 °C in the presence of 2 mM EDTA (Fig. 4), while 50 % activity was lost in 45 min at 37 °C. However, *Cm*AP was stable up to 45 °C with a half-life of 15 min at 47 °C and 120 min at 45 °C, when the enzyme was incubated with 10 mM $MgCl_2$ ($n=15$) (data not shown).

Upon dilution of a thousand fold, *Cm*AP was fully stable at −20 °C during more than 1-year storage in the dilution buffer (0.05 M Tris–HCl, pH 8.6, 0.01 % NaN_3).

Mg^{2+} Content of *Cm*AP

According to the results of atomic absorption spectrometry, only zinc and magnesium were found in the protein samples ($n=4$). The molar ratio of Mg^{2+} in *Cm*AP was determined as 1.2 ± 0.5.

Table 1 Isolation and purification of *Cm*AP

Step	Protein (mg)	Specific activity (U/mg)	Yield (%)
Cell homogenate	245	41	100
DEAE-cellulose-52	47.5	284	73
Ni-agarose	5	1,670	58
Enterokinase	5	1,650	57
Sephacryl S-100HR	2	3,800	34

The standard assay for AP activity was carried out in 0.1 M Tris–HCl buffer, 0.2 M KCl, 2 mM pNPP (pH 9.0) at 37 °C. The specific AP activity measured in 1 M DEA buffer and 20 mM pNPP (pH 10.3) at 37 °C

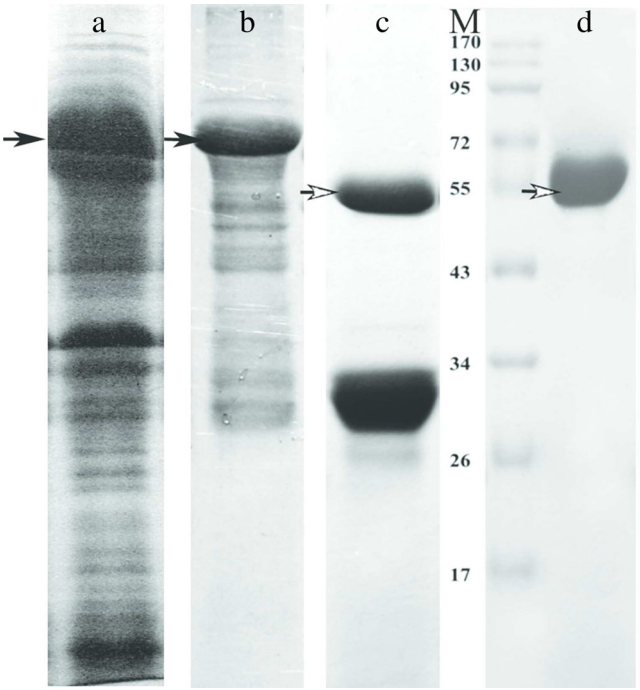

Fig. 1 SDS-PAGE of *Cm*AP: crude cell extract (*A*), enzymatic active fraction of hybrid recombinant protein 6xHis-DsbC-*Cm*AP from DEAE-Cellulose-52 (*B*), protein fraction eluted from Ni-NTA agarose and processed by enterokinase (*C*), and *Cm*AP eluted from Sephacryl S-100HR (*D*), Molecular weight marker (Bio-Rad) (*M*). *Black cursor* corresponds to hybrid recombinant protein 6xHis-DsbC-*Cm*AP (87 kDa). *Empty cursor* corresponds to *Cm*AP (55 kDa)

Effects of Chemicals on ***Cm*AP**

The incubation of *Cm*AP with 10–100 mM EDTA for 5 h decreased the activity only by 40 % (Fig. 5). The elution of *Cm*AP from Ni-agarose with 50 mM EDTA (pH 8.6) did not have any effect on the *Cm*AP activity, whereas the pre-incubation of the resin-bound *Cm*AP with 100 mM EDTA required the addition of 2 mM Mg^{2+} to retain 100 % of its activity (n=4) (data not shown). Incubation with 0.1–5 % of SDS decreased the *Cm*AP activity also by 40 %, indicating that *Cm*AP is SDS-resistant (n=6) (data not shown). PAGE of the native protein in the presence or absence of SDS followed by staining of the gels with the substrate yielded a single active band of *Cm*AP (data not shown). *Cm*AP was activated 2-fold by addition of 0.1–0.2 M of NaCl or KCl. Increase of NaCl concentrations more than 0.2 M resulted in a partial inactivation of *Cm*AP, whereas a slight increase of activation occurred even at 1 M KCl (Fig. 6).

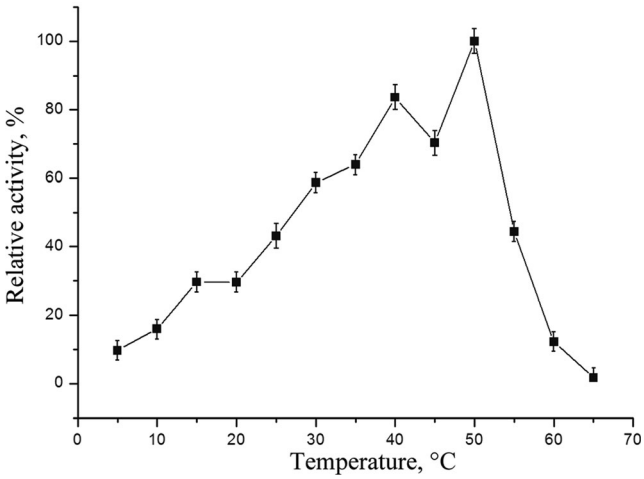

Fig. 3 Effect of temperature on activity of *Cm*AP. The enzyme activity was standard assayed (0.1 M Tris–HCl buffer, pH 9.0) using each temperature as the reaction temperature for 30 min (n=15, $p \leq 0.05$)

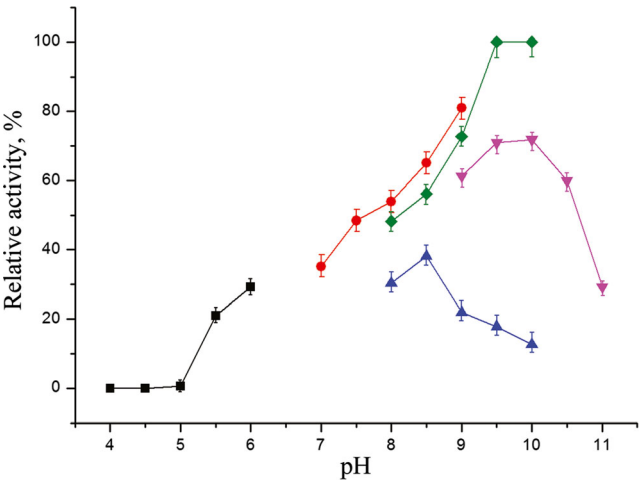

Fig. 2 Stability of *Cm*AP in different buffers. The enzyme activity was measured using the standard enzyme assay (0.1 M Tris–HCl buffer, pH 9.0) after 5-h incubation at different pH values. *Squares* indicate 0.03 M $NaCOOH_3$ (4.0–6.0), *circles* indicate 0.05 M Tris–HCl (7.0–9.0), *diamonds* indicate 1 M DEA (8.0–10.3), *down triangle* indicates 0.1 M $NaHCO_3$ (9.0–11.0), and *up triangle* indicates 0.1 M glycine (9.0–11.0) (n=9, $p \leq 0.05$)

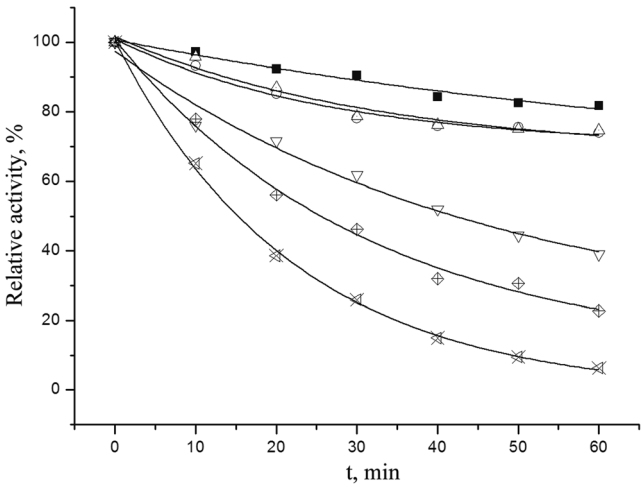

Fig. 4 Heat stability of *Cm*AP. The enzyme was incubated at the appropriate temperatures in the presence of 2 mM EDTA and the residual activity measured using the standard enzyme assay (0.1 M Tris–HCl buffer, pH 9.0) at 10 min intervals for 30 min. *Black squares* indicate 20 °C, *empty up triangle* indicates 25 °C, *empty circles* indicate 30 °C, *down triangle* indicates 37 °C, *crossed out diamond* indicates 40 °C, and *crossed out triangle* indicates 45 °C (n=9, $p \leq 0.05$)

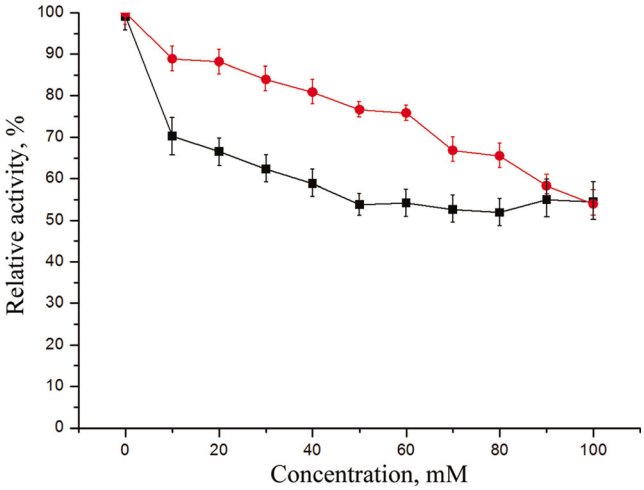

Fig. 5 Effect of EDTA on *Cm*AP activity and stability. The enzyme activity was measured using the standard assay with the addition of EDTA in the incubation mixture (*diamonds*); the enzyme was pre-incubated with EDTA concentration from 0 to 100 mM at 25 °C for 5 h and the residual activity measured using the standard enzyme assay (0.1 M Tris–HCl buffer, pH 9.0) (n=6, $p \leq 0.05$) (*squares*)

Kinetic Properties of *Cm*AP

Kinetic factors for *Cm*AP were determined under various conditions in 0.1 M Tris–HCl and 1 M DEA buffers at 25 °C, by varying pH values from 8.0 to 10.3. *Cm*AP had turnover number k_{cat}=28,300±2,100 s and Michaelis–Menten factor K_m=13.2±1.48 mM in 1 M DEA buffer with catalytic efficiency k_{cat}/K_m of 2.1×10^6 s/M for *p*NPP (Table 2). Catalytic efficiency and K_m value of *Cm*AP at pH 8.0 in 1 M DEA buffer were 8.2×10^7 s/M and 0.3 mM±0.02, respectively. *Cm*AP had lower catalytic parameters under all conditions in 0.1 M Tris–HCl buffers (Table 2).

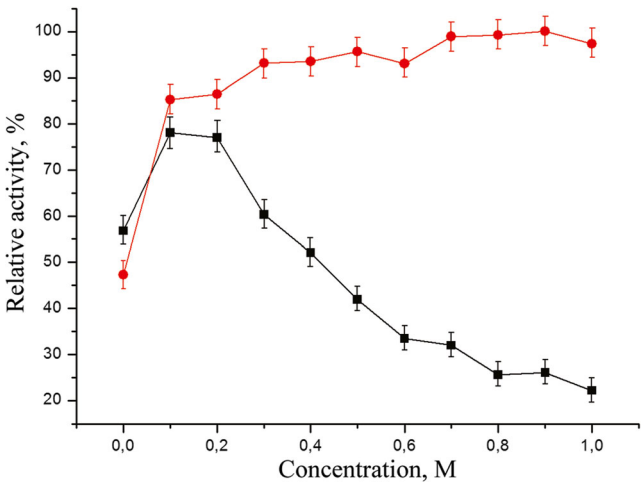

Fig. 6 Effect of Na^+ and K^+ on the *Cm*AP activity. Effect of NaCl (*squares*); effect of KCl (*circles*). The enzyme activity was standard assayed (0.1 M Tris–HCl buffer, pH 9.0) (n=6, $p \leq 0.05$)

Table 2 Kinetic factors of *Cm*AP at 25 °C

Buffer	k_{cat} (s)	K_m (mM)	k_{cat} (s/M)
DEA, pH 10.3	28,300±2,100	13.2±1.48	$2.1\times10^6\pm0.24\times10^6$
DEA, pH 8.0	24,000±1,520	0.3±0.02	$8.2\times10^7\pm0.55\times10^7$
Tris–HCl, pH 10.3	3,710±310	2.9±0.25	$1.2\times10^6\pm0.11\times10^6$
Tris–HCl, pH 8.0	1,500±280	0.045±0.008	$3.3\times10^7\pm0.5\times10^7$

The assay for AP activity was carried out in 0.1 M Tris–HCl buffer, 0.2 M KCl, pNPP 0.1–0.6 mM at pH 8.0, and 0.2–3.0 Mm at pH 10.3. The assay for AP activity measured in 1 M DEA buffer, pNPP 0.1–1.0 mM at pH 8.0, and 0.5–15 mM at pH 10.3. Table shows the data of ten experiments, confidence interval at $p \leq 0.05$

Primary Structure of *Cm*AP and Comparison with Other AP Sequences

The single AP gene consisting of 1,605 bp and encoding 535 amino acid residues (*aa*) of the AP precursor (accession no. DQ435608) was found in *C. marina*. A 32 *aa* signal sequence was identified that would direct the enzyme to the periplasmic space. The mature protein has a calculated molecular mass of 54,370 Da and an isoelectric point (p*I*) of 4.56, which are in a good agreement with experimental data (Plisova et al. 2005). The ORF had a G+C content of 56.64 % and encoded a high content of nonpolar and uncharged polar *aa,* such as Ala (11.33 %), Gly (8.75 %), Leu (8.55 %), Ser (6.76 %), Val (6.56 %), Thr (6.36 %), and negatively charged Asp (7.36 %). A search of the GenBank database disclosed the high identity (53–75 %) and similarity (69–86 %) of *Cm*AP to several explored and putative APs from marine γ-Proteobacteria, namely halophilic *Halomonas* sp. #593 (accession no. AB271127) and *Halomonas elongate* (FN869568), *Vibrio parahemoliticus* (BA000031), psychrophilic *Vibrio sp. G15-21* (AF352014), *Shewanella denitrificans* (CP000302), *Psychromonas ingrahamii* (AAQS01000001), and *Hahella chejuensis* (CP000155) (data not shown). Only the *Vibrio* G15-21 AP was completely biochemically and structurally evaluated (Hauksson et al. 2000; Helland et al. 2009). A relatively lower identity (≤38 %) and similarity (≤52 %) were observed for other APs, including AP from Antarctic bacterium TAB5 and mammalian and marine invertebrate APs (Rina et al. 2000; Le Du et al. 2001; De Backer et al. 2002; Kozlenkov et al. 2002).

Molecular Modeling and Site-Specific Mutagenesis of *Cm*AP

Alignment scores and stereochemical quality of the *Cm*AP models showed the *Vibrio* sp. G15-21 alkaline phosphatase (VAP) as the best template with 69.4 % identity and 82 % similarity (Fig. 7a). The *Cm*AP model building process was completed on the base of the high-quality experimental structure of VAP at 1.4-Å resolution (PDB code: 3E2D_A), showing that the bimetallo core structure was conserved (Fig. 7b).

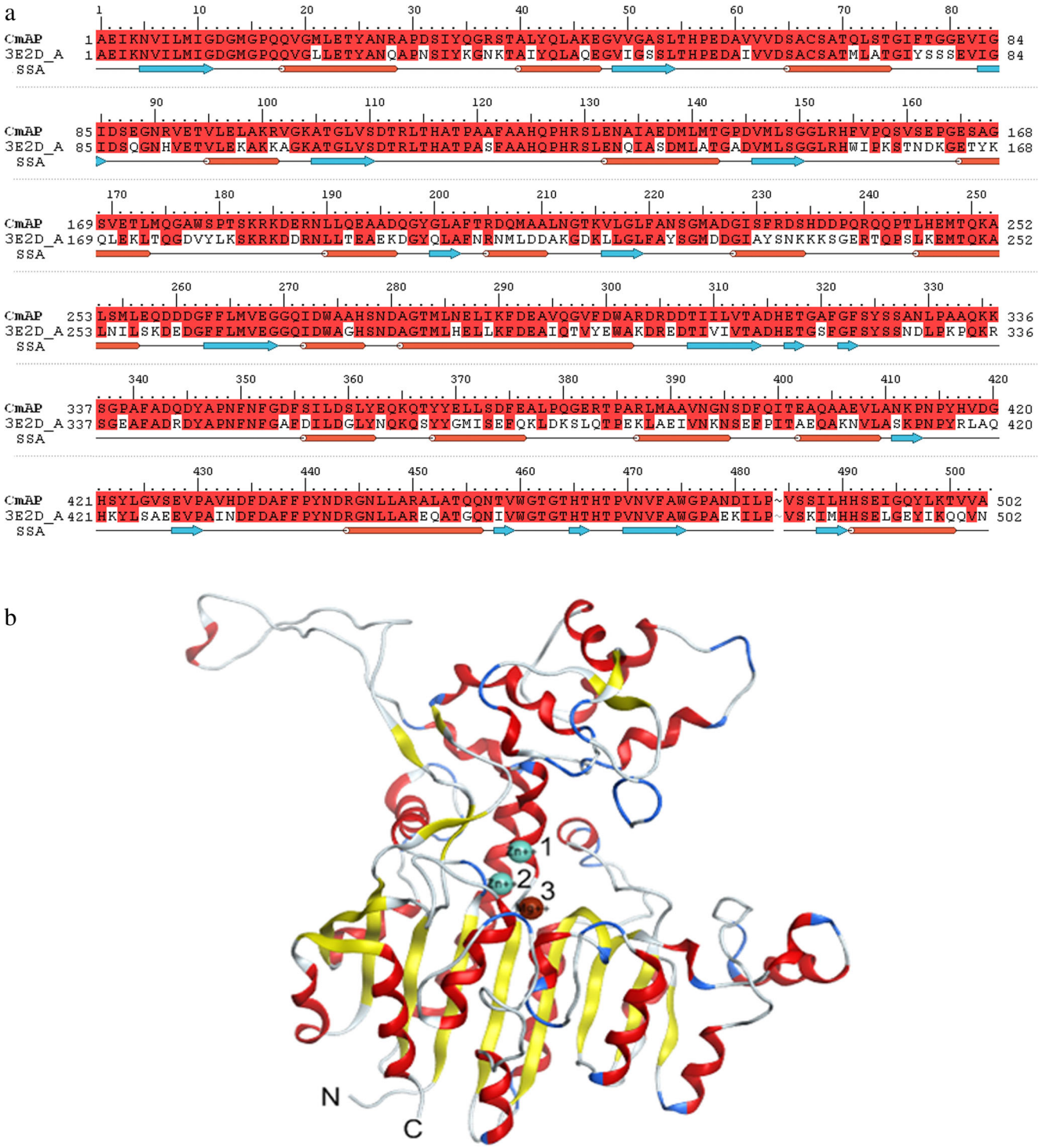

Fig. 7 **a** Sequence alignment of the alkaline phosphatase *Cm*AP from marine bacterium *C. marina* (UniProt: Q1W622) with template sequence of alkaline phosphatase VAP from marine bacterium *Vibrio* sp. G-15 (PDB code: 3E2D_A). Figure prepared with program Maestro 9.3. Secondary structure elements were shown for VAP. Identical and similar residues are shown with *red* and *orange colors*. **b** The 3D structure model of the alkaline phosphatase *Cm*AP monomer from marine bacterium *C. marina* built with the use of the crystal structure of VAP from marine bacterium *Vibrio* sp. G15-21 as template. Protein structure is shown as *ribbon diagram*. Secondary structure elements are β-strands (*yellow color*), α-helixes (*red color*), turns (*blue color*), and unordered structure (*gray color*). Metal ions Zn^{2+} (*1*), Zn^{2+} (*2*), and Mg^{2+} (*3*) are shown as *blue* and *brown spheres* (color figure online)

The Cα root mean square deviation (RMSD) value between *Cm*AP and VAP was calculated to be 0.43 Å. Although catalytic Ser65 and substrate-binding Arg129 and the residues bound with the metal ions were identical, the slight differences

were observed within the secondary structure. *Cm*AP has a higher content of α-helices and a lower content of β-strand elements than VAP does (Table 3). *Cm*AP displays a three-layer β-sandwich fold and contains β-sheet of nine β-strands surrounded by α-helices at both sides (α-β-α type). The *Cm*-AP structure is stabilized by 148 hydrogen bonds, 180 hydrophobic contacts, and 20 ionic bonds with the absence of disulfide bonds.

*Cm*AP had the same large "crown" domain and the long extension loops that cover the active site and can participate in the dimer formation as found in VAP (Fig. 7b) (Helland et al. 2009). However, the loop for the dimer stabilization (325–351 *aa*) was very movable depending on the molecular environment conditions (Figs. 7a and 8). As in the case of VAP, the *Cm*AP catalytic site was deeply buried in a crevice running between two loops. Although the overall molecular surface of *Cm*AP was largely hydrophobic, the calculation of the electrostatic surface potentials near the active site revealed the presence of a large extended surface of the positively charged *aa* along the narrow entrance to the enzymatic cave (Fig. 9). It may effectively cumulate the substrate molecules from the solution in the active center direction. On the other hand, the negatively charged *aa* located opposite the bound negatively charged P_i, facilitating its release from the active site (data not shown). A distinctive feature of the enzyme was also found by analysis of *Cm*AP protonation at various pH values. At the pH values ≥10.0, the substrate-binding Arg129 and the residue Tyr441 oriented toward the bound substrate become neutral and negatively charged, respectively (data not shown).

Estimates of binding strengths and specificities carried out for different ion types defined localization of two Zn^{2+} and one Mg^{2+} (data not show). In silico mutagenesis of *Cm*AP Mg^{2+}-binding site was carried out. The point mutations of the residues Asp12, Asp273, Asp315, His316, Thr118, Glu268, and Trp274 to Gly generated with program MOE showed that the Asp12Gly mutation should lead to the loss of ionic bonds of the residue with metal ions Zn_1, Zn_2, and Mg, hydrogen bonds Asp12.OD2-Ser65.OG, Asp12.OD2-Thr.OG1, and Asp12.OD1-His316.NE2 and hydrogen bonds with three water molecules in the active site, which are present in the Asp12 contacts (Fig. 10a, b). The Asp64Gly mutation led to the loss of ionic bond and hydrogen bond with Arg129 and hydrogen bonds with two water molecules in the active site, which are present in the Asp64 contacts (Fig. 10a, c). The Asp443Gly mutation led to the loss of hydrogen bond Asp443.OD2-Ser278.OG1 and hydrogen bonds with two water molecules, which are present in the Asp443 contacts (Fig. 10a, d). The Thr118Gly mutation led to the loss of hydrogen bond Thr118.OG1-Glu268.OE2 and hydrogen bonds with three water molecules in the active site, which are present in the Thr118 contacts (Fig. 10a, e). The Glu268Gly mutation led to the loss of ionic bond with Mg^{2+} and hydrogen bonds with two water molecules in the active site, which are present in the Glu268 contacts (Fig. 10a, f). The Asp315Gly mutation led to the loss of ionic bond Gly315 with ion Zn_2 and hydrogen bond with Gly13.N, which are present in the Asp315 contacts (Fig. 10a, g). The Trp274Gly mutation led to the loss of hydrogen bond with Ser278 and hydrogen bond with water molecule in the active site, which are present in the Trp274 contacts (Fig. 10a, h). The His316Gly mutation led to the loss of hydrogen bond His316.NE2-Asp12.OD1, which is present in the His316 contacts (Fig. 10a, i). The Asp273Gly mutation led to the loss of ionic bonds with ions Zn_1 and Zn_2 and hydrogen bond with Thr318.OG1, which are present in the Asp273 contacts (Fig. 10a, j). The substitution of Gly for the residues Asp12, Asp273, Asp315, His316, Tre118, Glu268, and Trp274 was also experimentally carried out in order to elucidate their role for the *Cm*AP activity. Where the interruption of the residue interaction with Mg^{2+} occurred, the enzymatic activity was completely lost, although the integrity of the molecular structure remained and only one or two hydrogen bounds were broken in the entire *Cm*AP hydrogen bond network (Fig. 10b, e–j). Only the enzymatic activity of Asp64Gly and Asp443Gly mutants, where the breaking of nonessential for Mg^{2+}-binding hydrogen bonds occurred in the periphery of the structure, was reduced 7-fold and 1/2-fold, respectively (Fig. 10c, d).

Molecular docking *Cm*AP with AMP has shown that the residue Trp274 localized near the active site entrance forms stacking interaction with the substrate ring that may facilitate the optimal space orientation of the substrate toward the active site, indicating specificity to DNA (Fig. 11). While docking with *p*NNP, the only PO_4^- connection in the *Cm*AP active site occurs (Figs. 9 and 11).

Discussion

It is evident that marine bacterial phosphatases possess unique properties that contribute greatly to living and functioning in oceanic waters. These enzymes appear to be distinct from their terrestrial counterparts in substrate preference, metal binding ligands, P_i affinity, thermostability, and catalytic efficiency.

Table 3 Content of the secondary structure elements in *Cm*AP and VAP

AP	β-Structure	α-Helix	α_{3-10}-Helix	Unordered structure
*Cm*AP model	69 (13.7 %)	188 (37.5 %)	19 (3.8 %)	226 (45.0 %)
Prototype VAP (PDB: 3E2D)	75 (14.9 %)	183 (36.5 %)	19 (3.8 %)	225 (44.8 %)

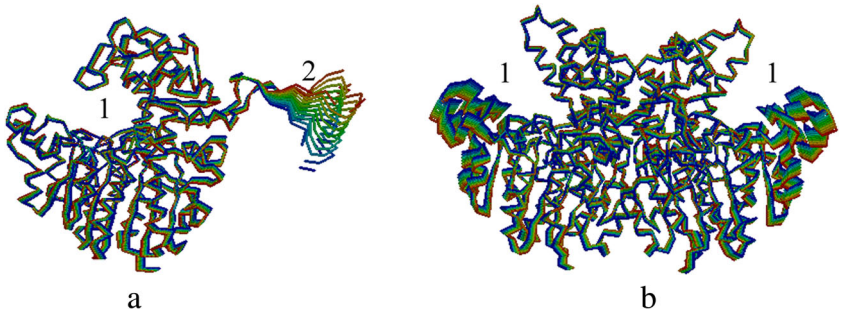

Fig. 8 Conformational flexibility of *Cm*AP. **a** Monomeric *Cm*AP: active centre (*1*) and the subunit loop stabilizing the dimer (*2*). **b** Dimeric *Cm*AP: active centers (*1*)

The marine bacterial APs such as the Antarctic psychrophile TAB5 (Rina et al. 2000), the psychrophile *Vibrio* G15-21 (Hauksson et al. 2000), the psychrophiles *Shewanella* sp. (Murakawa et al. 2002) and *Shewanella* sp. SIB1 (Suzuki et al. 2005), and the moderately halophilic *Halomonas* sp. 593 (Ishibashi et al. 2005) have been purified and biochemically studied. The activities of these enzymes are in the range of 427–3,707 U/mg. There is no comparison of the specific activity between the terrestrial and marine γ-Proteobacterial APs. The specific activity of native *E. coli* AP was approximately 60 U/mg, whereas the native *Cm*AP activity was approximately 14,000–15,000 U/mg (Plisova et al. 2005). Of the commercially available APs, the most active is the recombinant AP from bovine calf intestinal mucosa; it showed a specific activity of approximately 7,800 U/mg (Biozyme Laboratories). Currently, recombinant *C. marina* AP (*Cm*APase) was expressed by Nasu et al. (2012) using the synthetic gene adapted for *E. coli* and inserted in pET-16b(+) vector and had a specific activity of 12,700 U/mg, which is the highest activity reported for any bacterial or mammalian AP. The specific activity and catalytic efficiency of our recombinant enzyme (*Cm*AP) produced in *E. coli* on the base of the nature gene of *C. marina* and pET-40b(+) vector were also the highest among any of the APs studied to date (Tables 1 and 2). The kinetic parameters of *Cm*AP were 0.3–13.2 mM (K_m) and 24,000–28,300 s (k_{cat}) with the catalytic efficiency of 2.1×10^6–8.2×10^7 s/M (Table 2). For comparison, the K_m of *E. coli* AP was 0.06 mM and a k_{cat} of 62 s with the catalytic efficiency of 1.1×10^6, whereas the K_m of bovine intestinal AP, including its catalytically improved mutants, ranged from 1.3 to 3.9 mM and the k_{cat} ranged from 1,800 to 6,100 s with the catalytic efficiency of $1.4–1.6\times10^6$ s/M (Hauksson et al. 2000; Kozlenkov et al. 2002).

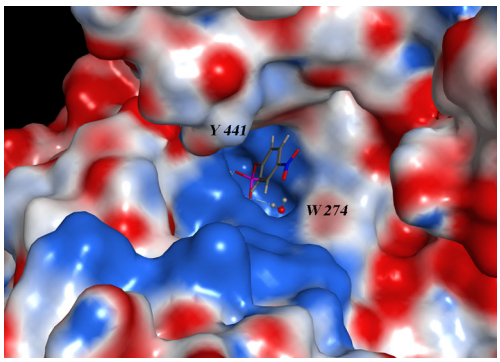

Fig. 9 Electrostatic neighbored surface potentials of *Cm*AP active site bound with substrate *p*NNP. Positively charged amino acid residues are indicated by *blue color*. Negatively charged amino acid residues are indicated by *red color* (color figure online)

Surprisingly, the native *C. marina* AP signal peptide was found to be appropriate for *E. coli* system to produce periplasmic recombinant protein (Nasu et al. 2012). Alternatively, the use of *E. coli* signal peptide included in the expression plasmid pET40b(+) resulted in overproduction of the soluble highly active *Cm*AP (Table 1). It should be noted that removing of the N-terminal His-tag and 32.5 kDa DsbC parts from the hybrid protein 6xHis-DsbC-*Cm*AP could be optional due to the absence of their effect on the *Cm*AP activity (Fig. 1). However, the recombinant plasmid pET22b(+) containing the mature *Cm*AP sequence and a C-terminal 6xHis tag produced *Cm*AP in body inclusion despite of the presence of N-terminal *E. coli* leader (data not shown). The additional C-terminal His-tag sequence probably decreased the *Cm*AP solubility. The hydrophobic tail of native *Cm*AP may be required to prevent secretion of the enzyme into the sea medium or to participate in protein folding (Kim et al. 1998). It was reported that natural marine bacteria have a cell surface phosphatase-like enzyme that rapidly hydrolyses 5′-nucleotides and regenerates P_i, increasing its uptake while decreasing the concentration of P_i in the environment (Ammerman and Azam 1985).

From our data, the relative molecular mass of *Cm*AP evaluated by native-PAGE, SDS-PAGE, and gel filtration column chromatography under pH 8.6 was to be 55,000 Da, suggesting the one-subunit molecular organization of the enzymatically active *Cm*AP under the experimental conditions. However, the gel permeation of a recombinant *C. marina* AP (*Cm*APase) carried out by Nasu et al. (2012) at pH 10.0 resulted in the formation of the enzyme dimer. It seems probable that more flexible links at the dimer interface of the cold-adapted enzymes may ease the structural rearrangement and thereby facilitating more rapid release of phosphate and thus catalytic turnover (Asgeirsson et al. 2003). Most known APs are active as homodimeric metalloenzymes that contain zinc and magnesium ions. Their active site pockets are conserved with the exception of a few key residues directly or

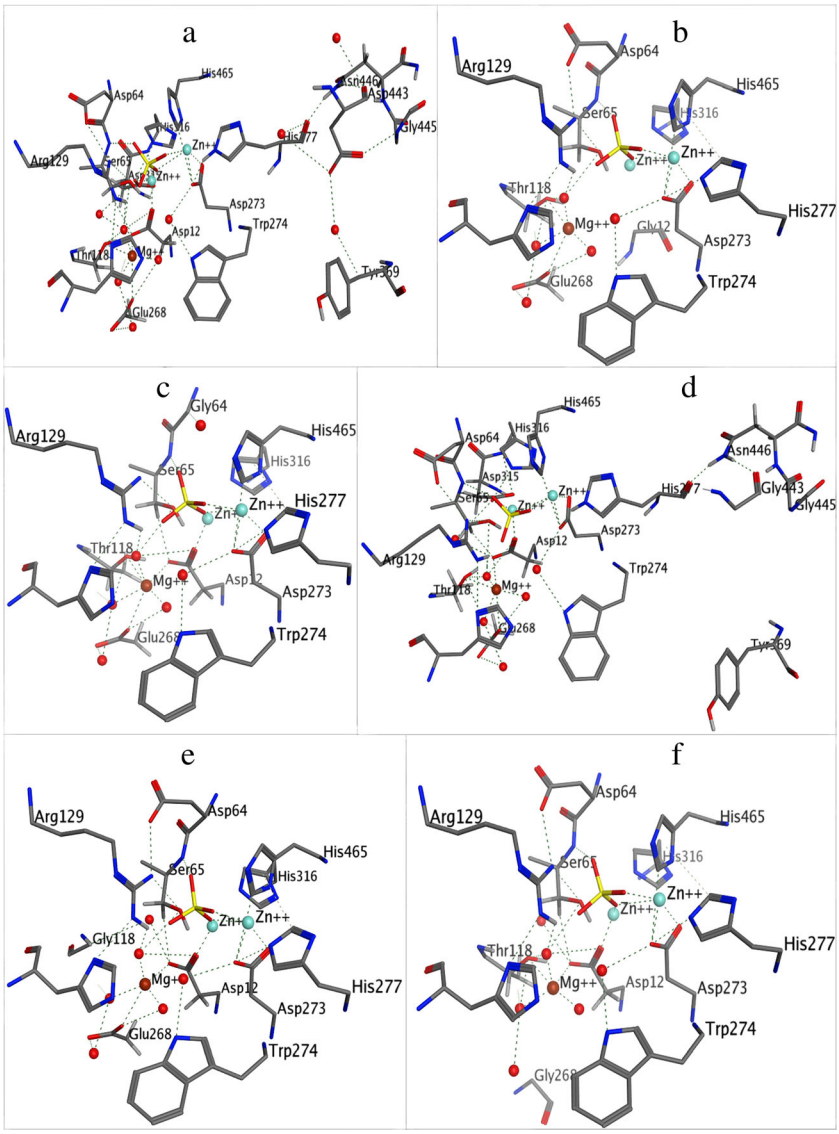

Fig. 10 **a**, **b**, **c**, **d**, **e**, **f** Atomic detailed structures of *Cm*AP active center and metal-binding sites (**a**) and its mutants Asp12Gly (**b**), Asp64Gly (**c**), Asp443Gly (**d**), Thr118Gly (**e**), and Glu268Gly (**f**) in silico generated with MOE 2012.10. The coordinates of the metal ions and sulfate ion produced by superposition model *Cm*AP with crystal structure of VAP. Water is shown as *red sphere*. Metal ions Zn^{2+} (1), Zn^{2+} (2), and Mg^{2+} (3) were shown as *blue* and *brown spheres*. **g**, **h**, **i**, **j** Atomic detailed structures of the active center and metal-binding sites of *Cm*AP mutants Asp315Gly (**g**), Trp274Gly (**h**), His316Gly (**i**), and Asp273Gly (**j**) in silico generated with MOE 2012.10. The coordinates of the metal ions and sulfate ion produced by superposition *Cm*AP model with crystal structure of VAP. Water is shown as *red sphere*. Metal ions Zn^{2+} (1), Zn^{2+} (2) and Mg^{2+} (3) were shown as *blue* and *brown spheres* (color figure online)

indirectly involved in the coordination of the metal ion in the third ion binding site (M3), which is normally occupied by magnesium (Zalatan et al. 2008). A few APs have been reported to be monomeric, and some have been reported that were stable as a monomer but not active (Hulett et al. 1991; Hauksson et al. 2000; Zappa et al. 2001). Interestingly, *Sphingomonas* sp. AP (SPAP) was eluted as an active monomer in size exclusion chromatography experiments, although crystal formation results in visualization of a dimer (Bihani et al. 2011). It has been suggested that the dimerization found in the crystals is a crystallization artifact because surface area buried upon dimerization is lower than in other AP's. Distinct from the majority of known APs, the marine γ-Proteobacterial AP dimer formation was archived by another mechanism. Introduction of bulky side chains in the subunit interface on two additional inserts contributed to VAP dimer formation (Helland et al. 2009). The absence of the stabilizing N-terminal helix, which is found in other APs, was compensated for by additional *aa* inserts. *Cm*AP model showed the same large crown domain and the long extension loops that cover the active site and can connect the monomers. The *Cm*AP 3D structure was predicted by the homology modeling approach owing to availability of a highly homologous VAP crystal structure as the only 3D structure of a marine γ-

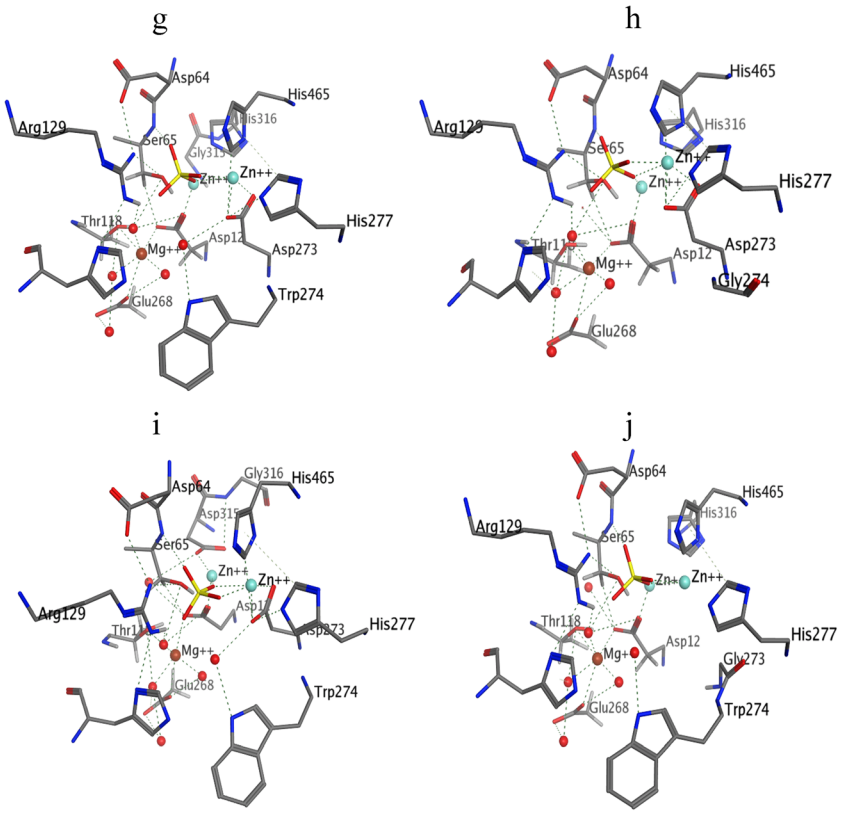

Fig. 10 (continued)

Proteobacterial AP (Fig. 7). Current approach to refining protein structure models with templates from the Protein Data Bank (PDB) can significantly improve the accuracy of the structures providing often better solutions to the X-ray crystallographic phase problem (Qian et al. 2007; Moult 2007). Although catalytic Ser65 and substrate-binding Arg129 and the residues bound with the metal ions Zn_1, Zn_2 and Mg in *Cm*AP and VAP were identical, the slight differences were observed within the primary and secondary structures. The analysis of nonidentical *aa* region that was predominantly found on the molecular surfaces of the compared proteins showed an increase from 2- to 10-fold in Ala, Val, Arg, Pro, Gly, and Phe and otherwise decrease in Lys, Ile, Asn, and Tyr in *Cm*AP (Fig. 7a). In addition, *Cm*AP had 2 % difference in the content of the secondary structure elements and hydrophobic *aa* covering molecular surface (Table 3, Fig. 7a). The minor structural differences in *Cm*AP and VAP probably define the apparent differences in their properties. *Cm*AP exhibited 4- and 1/2-fold higher thermal stability with a half-life of 27 min versus the VAP half-life of only 6 min at 40 °C (Fig. 4) (Hauksson et al. 2000). Heat stability was increased up to 120 min at 45 °C for the loss of 50 % of the *Cm*AP initial activity in the presence of stabilizer Mg^{2+} (data not shown). Although *Cm*APase had lower activity than *Cm*AP that could be the result of the recombinant production method (Nasu et al. 2012). *Cm*AP is more close to AP from moderate halophile *Halomonas* sp. 593 (HaALP) as judged by the *aa* sequence (75 % identity, 86 % similarity) as well as thermostability and halotolerance (Ishibashi et al. 2005).

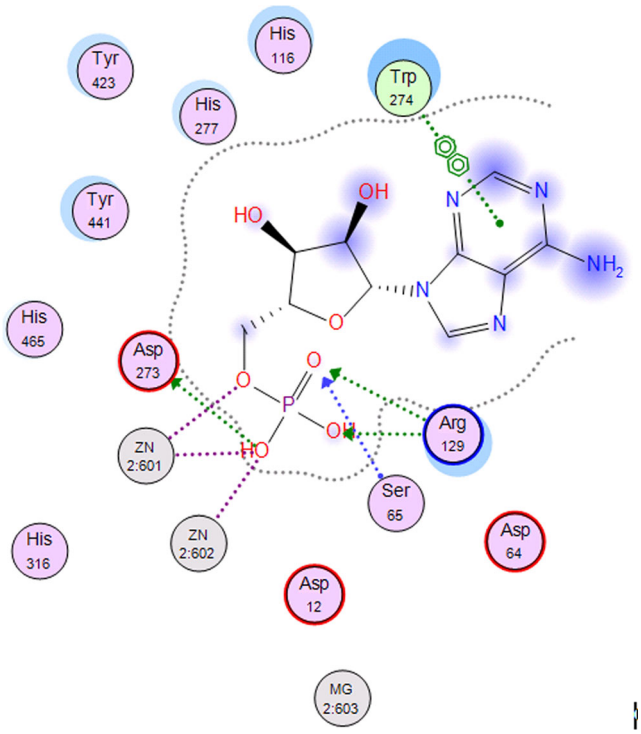

Fig. 11 Diagram of contacts of the substrate AMP interactions in *Cm*AP active site

However, in distinction from HaALP, KCl was more effective than NaCl for activation and stabilization of *Cm*AP, suggesting the importance of K^+ ions for the *Cm*AP functioning environment (Fig. 6). The important role of K^+ in apoptose and proliferation of cells in mineralized tissues that are under continuous renewal was recently determined (Page and Di Sera 2006; Henney et al. 2009).

It is probable that the structural features of the *Cm*AP active site provide a barrier to prevent contact of denaturants, including chelators, with the active site. Metal ions released from the active site by heat or pre-incubation with EDTA in high concentrations for long time only led to decrease of enzymatic activity (Figs. 3, 4, and 5). These may coincide with the loss of the magnesium ion from the active site because of increased mobility of the binding ligands (Gudjónsdóttir and Asgeirsson 2008). However, *Cm*AP retained its stability and activity after pre-incubation with EDTA in concentration of 50–100 mM in the presence of Mg^{2+} (data not shown). It has been suggested that *Cm*AP does not require an excess of Mg^{2+} for binding in the M3 site, which has been generally noticed in the structural reorganization that occurs upon metal binding during enzyme dimerization and activation (Janeway et al. 1993; Poltorak et al. 1999; Babor et al. 2005). The high working efficacy and stability of a monomeric *Cm*AP can be attributed to the intrinsically tight binding of both catalytic and structural metal ions. Strong metal–enzyme interactions in the AP active site have been reported (Zappa et al. 2001; Zaheer et al. 2009). Estimates of binding strengths and specificities of metal ions using the *Cm*AP 3D structure model and atomic absorption analysis confirmed two zinc and one magnesium ions and their ligands in the active site (Figs. 7 and 10). However, the existence of the additional Mg^{2+}-binding sites with possible functional role in *Cm*AP may well be true considering the effect of exogenous Mg^{2+} on the *Cm*AP thermal stability.

Amino acid residues that interact with the zinc ions in the M1 and M2 sites of APs are conserved in all known sequences. His116 and Trp274 occurred near the Mg^{2+}-binding site (M3) and identified in *Cm*AP have been mutated in VAP (Gudjónsdóttir and Asgeirsson 2008). The structural study of the *Cm*AP mutants with the predicted removal of the Mg^{2+} site revealed differences in metal coordination. Remarkably, given its large detrimental effect on the substrate hydrolysis, mutation of the *Cm*AP that predicted Mg^{2+}-binding ligands to Gly appears to be linked to more general structural factors (Fig. 10). Each intermolecular Mg^{2+} contact is directly or indirectly implicated in all metal ion coordination and included in the unified hydrogen bond network penetrated through the entire molecular structure. The alteration in the metal coordination is directly related to alterations of P_i affinity in the active site of the enzyme (Wang et al. 2007). Furthermore, a little or no cooperativity between the substrate-binding Arg and the Mg^{2+} site in their contributions to catalysis has been found (Zalatan et al. 2008). It could explain the drastic increase in catalytic turnover and K_m at pH≥10.0 in *Cm*AP (Table 2). When the Mg^{2+} ion stabilization effect on the transferred phosphoryl group and the Zn^{2+} bimetallo site interactions remained, the residue Arg129 became neutral (Figs. 10 and 11). As the release of P_i is the slow step in the mechanism at alkaline pH, the weakened binding of P_i together with the additional negatively charged Tyr441 at a high pH should contribute to rapid release of negatively charged product from the *Cm*AP active center. This increases not only K_m but also catalytic turnover (k_{cat}) many times. However, catalytic efficiency of *Cm*AP was higher at pH 8.0 in 1 M DEA buffer because the enzyme had a significantly lower K_m value (Table 2). Remarkably, the residue Tyr367 is part of the subunit interface in the human placenta AP (PLAP) dimer, where it protrudes from one subunit and its hydroxyl group is located 6.1 Å from the phosphate and 3.1 Å from His432, which in turn chelates the zinc atom Zn_1 in the active site of the other subunit, playing a crucial role in determining the allosteric character of PLAP (Millan 2006). Tyr325 from the VAP B-subunit extends into the A-subunit substrate-binding site with the hydroxyl group 4.69 Å from Zn at the M1 position (Helland et al. 2009). However, the residue Tyr441 also protrudes above the *Cm*AP active site entrance and may play analogous role for functioning as monomer (Fig. 9).

Although APs catalyze the hydrolysis of a wide variety of phosphomonoesters at similar rates, *Cm*AP prefers substrates such as *p*NPP, 5′-AMP, 5′-CMP, α-glycerophosphate (Plisova et al. 2005). The narrowest specificity was found in APs from mammalian sources. Distinct from bacterial APs, the calf intestinal AP only catalyzes the hydrolysis of *p*NPP and 5′-AMP at a high rate, whereas all other substrates are cleaved much slower (McComb et al. 1979). It is evident that the rate of hydrolysis with *Cm*AP decreases with the increase of the size of the substrate molecular due to the narrow entrance into the active site (Figs. 9 and 11). However, *Cm*AP was found to hydrolyze DNA effectively as well as the current luminescent substrates used in the majority of the AP methods (Plisova et al. 2005; Nasu et al. 2012).

It is evident that *Cm*AP is an example of structural alterations in APs adapted to function in the marine environment. Taking advantage of enzymatic properties that nature has evolved, *Cm*AP can be used in a number of biotechnology approaches. A relatively low thermostability can be useful for AP removing from the reaction mixture without additional purification in DNA techniques (Plisova et al. 2005). A high specific activity value under transphorylation conditions and the metal-cofactor independence as well as the monomeric station of AP can be useful for rapid monitoring and optimization of various aspects of recombinant protein production by tagging AP to the protein of interest via genetic fusion (unpublished data). Similarly, a broad pH stability and a high stability against chelate agents can be useful in recombinant protein purification. The feasibility of using the genetic

fusions of AP monomer with peptides and proteins as a dual functional tag, as both an affinity tag and as a label in the development of an enzymatic assay to detect a ligand of interest, can be used in clinical diagnostics (unpublished data).

In summary, the detailed experimental and theoretical/computational investigations of marine *Cm*AP suggest that their advances in structural arrangement, biochemical properties, and catalytic efficacy can be successfully used in such practical applications as immunoassay systems, Southern blotting, Western blotting, reporter gene assays, and ELISAs. Based on the understanding of the enzyme structure and function, it may be possible to design more efficient enzymes or enzymes with novel functionalities. This knowledge may have wide implications in enzyme engineering as well as drug design.

Acknowledgments The work was supported by grant from RFBR 12-04-00825-a and the projects 13 НТПП-12, 12-I-П6-10.

References

Ammerman JW, Azam F (1985) Bacterial 5'-nucleotidase in aquatic ecosystems: a novel mechanism of phosphorus regeneration. Science 227:1338–1340

Aono T, Maldonado-Mendoza IE, Dewbre GR, Harrison MJ, Saito M (2004) Expression of alkaline phosphatase genes in arbuscular mycorrhizas. New Phytol 162:525–534

Asgeirsson B, Nielsen BN, Hojrup P (2003) Amino acid sequence of the cold-active alkaline phosphatase from Atlantic cod (*Gadus morhua*). Comp Biochem Physiol B Biochem Mol Biol 136:45–60

Babor M, Greenblatt HM, Edelman M, Sobolev V (2005) Flexibility of metal binding sites in proteins on a database scale. Proteins 59:221–230

Bihani SC, Das A, Nilgiriwala KS, Prashar V, Pirocchi M, Apte SK, Ferrer JL, Hosur MV (2011) X-Ray structure reveals a new class and provides insight into evolution of alkaline phosphatases. PLoS One 6:e22767

Bradford MM (1976) A rapid and sensitive method for the quantitation of microgram quantities of protein-dye binding. Anal Biochem 72: 248–254

De Backer M, McSweeney S, Rasmussen HB, Riise BW, Lindley P, Hough E (2002) The 1.9 A crystal structure of heat-labile shrimp alkaline phosphatase. J Mol Biol 318:1265–1274

Dell'Anno A, Danavaro R (2005) Extracellular DNA plays a key role in deep-sea ecosystem functioning. Science 309:2179

Dorozhkin SV (2009) Calcium orthophosphates in nature, biology and medicine. Materials 2:399–498

Gudjónsdóttir K, Asgeirsson B (2008) Effects of replacing active site residues in a cold-active alkaline phosphatase with those found in its mesophilic counterpart from *Escherichia coli*. FEBS J 275:117–127

Hauksson BJ, Andresson OS, Asgeirsson B (2000) Heat-labile bacterial alkaline phosphatase from a marine *Vibrio* sp. Enzyme Microb Technol 27:66–73

Helland R, Larsen RL, Asgeirsson B (2009) The 1.4 A crystal structure of the large and cold-active *Vibrio* sp. alkaline phosphatase. Biochim Biophys Acta 1794:297–308

Henney NC, Li B, Elford C, Reviriego P, Campbell AK, Wann KT (2009) A large-conductance (BK) potassium channel subtype affects both growth and mineralization of human osteoblasts. Am J Physiol Cell Physiol 297:1397–1408

Hess B, Kutzner C, van der Spoel D, Lindahl E (2008) GROMACS 4: algorithms for highly efficient, load-balanced, and scalable molecular simulation. J Chem Theory Comp 4:435–447

Hoppe HG (2003) Phosphatase activity in the sea. Hydrobiologia 493: 187–200

Hulett FM, Kim EE, Bookstein C, Kapp NV, Edwards CW, Wyckoff HW (1991) Bacillus subtilis alkaline phosphatases III and IV. Cloning, sequencing, and comparisons of deduced amino acid sequence with *Escherichia coli* alkaline phosphatase three-dimensional structure. J Biol Chem 266:1077–1084

Ishibashi M, Yamashita S, Tokunaga M (2005) Characterization of halophilic alkaline phosphatase from *Halomonas* sp. 593, a moderately halophilic bacterium. Biosci Biotechnol Biochem 69:1213–1216

Ivanova EP, Christen R, Sawabe T, Alexeeva YV, Lysenko AM, Chelomin VP, Mikhailov VV (2005) Presence of ecophysiologically diverse populations within cobetia marina strains isolated from marine invertabrate, algae and the environments. Microb Environ 20:200–207

Janeway CM, Xu X, Murphy JE, Chaidaroglou A, Kantrowitz ER (1993) Magnesium in the active site of *Escherichia coli* alkaline phosphatase is important for both structural stabilization and catalysis. Biochemistry 32:1601–1609

Kim JW, Peterson T, Bee G, Hulett FM (1998) Bacillus licheniformis MC14 alkaline phosphatase I gene with an extended COOH-terminus. FEMS Microbiol Lett 159:47–58

Kobori H, Sullivan CW, Shizya H (1984) Heat-labile alkaline phosphatase from Antarctic bacteria: rapid 5'-end-labeling of nucleic acids. Proc Natl Acad Sci U S A 81:6691–6695

Kozlenkov A, Manes T, Hoylaerts MF, Millan JL (2002) Function assignment to conserved residues in mammalian alkaline phosphatases. J Biol Chem 277:22992–22999

Laemmli UK (1970) Cleavage of structural proteins during the assembly of thehead of the bacteriophage T7. Nature 227:80–685

Le Du MH, Stigbrand T, Taussig MJ, Menez A, Stura EA (2001) Crystal structure of alkaline phosphatase from human placenta at 1.8 A resolution. Implication for a substrate specificity. J Biol Chem 276:9158–9165

Leveque I, Cusack M, Davis SA, Mann S (2004) Promotion of fluorapatite crystallization by soluble-matrix proteins from *Lingula Anatina* shells. Angew Chem Int Ed Engl 43:885–888

Li H, Robertson AD, Jensen JH (2005) Very fast emperical prediction and interpretation of protein pKa values. Proteins 61:704–721

McComb RB, Bowers GN, Posen S (1979) Alkaline phosphatase. Plenum Press, NY

Millan JL (2006) (2006) Alkaline phosphatases structure, substrate specificity and functional relatedness to other members of a large superfamily of enzymes. Purin Sign 2:335–341

Moult J (2007) Comparative modeling in structural genomics. Structure 16:14–16

Murakawa T, Yamagata H, Tsuruta H, Aizono Y (2002) Cloning of cold-active alkaline phosphatase gene of a psychrophile, *Shewanella* sp., and expression of the recombinant enzyme. Biosci Biotechnol Biochem 66:754–761

Nasu E, Ichiyanagi A, Gomi K (2012) Cloning and expression of a highly active recombinant alkaline phosphatase from psychrotrophic Cobetia marina. Biotechnol Lett 34:321–8

Olsson MHM, Søndergard SR, Rostkowski M, Jensen JH (2011) PROPKA3: Consistent treatment of internal and surface residues in empirical pKa predictions. J Chem Theory Comp 7:525–537

Paerl HW, Merkel SM (1982) Differential phosphorus assimilation in attached vs. unattached microorganisms. Arch Hydrobiol 93:125–134

Page MJ, Di Sera E (2006) Role of Na+ and K+ in enzyme function. Physiol Rev 86:1049–1092

Plisova EY, Balabanova LA, Ivanova EP, Kozhemyako VB, Mikhailov VV, Agafonova EV, Rasskazov VA (2005) A highly active alkaline phosphatase from the marine bacterium *Cobetia*. Mar Biotechnol 7: 173–178

Poltorak OM, Chukhray ES, Torshin IY, Atyaksheva LF, Trevan MD, Chaplin MF (1999) Catalytic properties, stability and the structure of the conformational lock in the alkaline phosphatase from *Escherichia coli*. J Mol Catalys B 7:165–172

Qian B, Raman S, Das R, Bradley P, McCoy AJ, Read RJ, Baker D (2007) High-resolution structure prediction and the crystallographic phase problem. Nature 450:259–261

Rahmanov S, Kulakovskiy I, Uroshlev L, Makeev V (2010) Empirical potentials for ion binding in proteins. J Bioinform Comput Biol 8: 427–435

Rina M, Pozidis C, Mavromatis K, Tzanodaskalaki M, Kokkinidis M, Bouriotis V (2000) Alkaline phosphatase from the Antarctic strain TAB5. Eur J Biochem 267:1230–1238

Sambrook J, Fritsch EF, Maniatis T (1989) Molecular cloning: a laboratory manual, 2nd edn. Cold Spring Harbor Laboratory Press, Cold Spring Harbor, NY

Suzuki Y, Mizutani Y, Tsuji T, Ohtani N, Takano K, Haruki M, Morikawa M, Kanaya S (2005) Gene cloning, overproduction, and characterization of thermolabile alkaline phosphatase from a psychrotrophic bacterium. Biosci Biotechnol Biochem 69:364–373

Van der Spoel D, Lindahl E, Hess B, Groenhof G, Mark AE, Berendsen HJC (2005) GROMACS: fast, flexible and free. J Comp Chem 26: 1701–1718

Van der Spoel D, Lindahl E, Hess B, and the GROMACS development team, GROMACS User Manual version 4.6.3 (2013), www.gromacs.org

Wang E, Koutsioulis D, Leiros HK, Andersen OA, Bouriotis V, Hough E, Heikinheimo P (2007) Crystal structure of alkaline phosphatase from the antarctic bacterium TAB5. J Mol Biol 366: 1318–1331

Zaheer R, Morton R, Proudfoot M, Yakunin A, Finan TM (2009) Genetic and biochemical properties of an alkaline phosphatase PhoX family protein found in many bacteria. Environ Microbiol 11:1572–87

Zalatan JG, Fenn TD, Herschlag D (2008) Comparative enzymology in the alkaline phosphatase superfamily to determine the catalytic role of an active-site metal ion. J Mol Biol 384:1174–1189

Zappa S, Rolland J-L, Flament D, Gueguen Y, Boudrant J, Dietrich J (2001) Characterization of a highly thermostable alkaline phosphatase from the euryarchaeon *Pyrococcus abyssi*. Appl Environ Microbiol 67:4504–4511